Polyelectrolyte Electrophoresis in a Dilute Solution of Neutral Polymers: Model Studies

Margaret E. Starkweather, David A. Hoagland,* and M. Muthukumar

Department of Polymer Science and Engineering and Materials Research Science and Engineering Center (MRSEC), University of Massachusetts Amherst, Amherst, Massachusetts 01003

Received July 16, 1999; Revised Manuscript Received December 20, 1999

ABSTRACT: Dilute neutral polymer solutions provide an effective environment for the electrophoretic separation of polyelectrolytes by molecular weight. To better understand the mechanisms responsible, this study examines how the molecular weight dependent mobility μ of poly(styrenesulfonate), termed the probe chain, depends on the molecular weight and concentration of various dilute pullulans, termed the host chains. Available for this system are nearly monodisperse probes and hosts. Carefully performed capillary electrophoresis experiments measure absolute values of μ and its distribution. Below the overlap concentration, hosts reduce μ from its free solution value in proportion to concentration. The strongest dependence of μ on probe molecular weight occurs at nearly equal probe and host chain lengths. The influence of host and probe chain lengths on μ can be understood in terms of pairwise probe−host configurational interactions. Three parameters—entanglement probability, average entanglement duration, and average entanglement displacement—capture the interaction dynamics and help to explain observed variations in μ.

Introduction

Advantages of speed, reproducibility, and precision have driven the rapid spread of analytical methods based on capillary electrophoresis (CE). An ability to accommodate a fluidlike separation medium is an equally important benefit to CE. Unfortunately, electrophoresis of charged polymeric solutes in a simple liquid containing small ions—the simplest fluid environment—does not provide any molecular weight discrimination. In contrast, CE in neutral polymer solutions can fractionate polymeric solutes by molecular weight nearly as well as traditional slab gels, an ability apparently first noted by Bode.[1,2] High-resolution analyses of DNA restriction fragments and poly(styrenesulfonate) (PSS) molecular weight standards, for example, have been accomplished in un-cross-linked solutions of linear hydroxyethylcellulose, methylcellulose, hydoxypropylcellulose, dextran, and poly(ethylene oxide).[3−16] Our understanding of the separation mechanism(s) in fluidlike environments remains less satisfactory than our understanding of these mechanisms in solid media such as gels. To gain fundamental insights that could help in the development and testing of molecular level models, we report here on the electrophoretic mobility μ of dilute, nearly monodisperse polyelectrolytes migrating through a dilute solution of a nearly monodisperse neutral polymer at concentration c (in units of mass/volume). The mobile polyelectrolyte, PSS, and the neutral matrix polymer, pullulan, are termed the "probe" and "host", respectively. In our model studies, probe molecular weight M and host molecular weight N are varied systematically over broad ranges.

Most theories for gel electrophoresis invoke gel mesh spacings or pore sizes to explain discrimination of probes by M. Below the critical overlap concentration c^*, one cannot readily envisage the presence of even a transient network or pore structure in a polymer solution, so new arguments must be advanced for dilute solution CE to explain how migrating chains are separated by size. To better understand the phenomenon, investigators have examined some of the factors affecting separation in neutral polymer solutions of various concentration, for example, by experimentally addressing trends in μ with probe and host molecular weight[8,14,16−18] as well as host concentration,[14,16,17,19−21] polydispersity,[17] and hydrophilicity/solvent quality/chain stiffness.[16] No literature report, however, has provided the unambiguous and quantitative experimental information needed to frame and test theory. Here, we provide such information for highly flexible, heavily charged polymers separated in dilute neutral polymer solutions.

Our specific goal is to investigate the interplay between M and N in the regime of dilute hosts. This goal mandates the systematic employment of nearly monodisperse hosts and probes. In the literature discussing CE with neutral polymers, the polydispersity index (PDI) for host polymers, defined by the ratio of weight- to number-average chain length, has rarely been reported. We are unaware of any studies with dilute hosts in which the host PDI could have been less than 2. Reported values of host PDI have ranged between 5 and 12.[17,21] Notwithstanding their use of polydisperse hosts, previous investigators have established a crucial role for N. In crude terms, "high" N hosts better separate "large" M probes, while "low" N hosts better separate "small" M probes.[7,8,14,17,18,20,22] The same trends hold for semidilute or concentrated host solutions.[16] In at least some cases, mixing of large and small hosts has been demonstrated to increase the effective range of probe separation by M.[6,17,23]

Barron et al. advanced the first molecular level explanation for the electrophoretic separation of polyelectrolytes in dilute neutral polymer solutions.[8,20,21] This explanation, termed transient entanglement coupling, proposes that "collisions" between probe and host(s) generate probe−host entanglements that effectively delay the probe's average field-induced drift. Although the concept has much appeal, transient entanglement coupling presents considerable ambiguity in specific details. Some investigators argue that the local resis-

10.1021/ma9911546 CCC: $19.00 © 2000 American Chemical Society
Published on Web 01/25/2000

tance of a host solution depends on the average number of immobile hosts in contact with the probe as well as N,[24] while others postulate that the enhanced retardation of large M probes by larger N hosts results from an evolution from collision at the host surfaces to collision after permeation.[18] Visualizations of DNA trajectories during electrophoretic motion in dilute host solutions reveals "waltzing" motion and V- or U-shaped chain configurations,[25,26] while electric birefringence and dichroism work sensitive to chain orientation suggests the importance of 1−1 probe−host complexes.[27,28] We recently performed Monte Carlo simulations to better understand the probe−host interaction and found complex configurational dynamics, even when considering only a single probe and host.[29,30] At moderate electric fields, the most significant probe−host configuration is a field-oriented "double hairpin" that vanishes as the shortest hairpin arm retracts through the locus of entanglement; this arm can belong to either probe or host, with a statistical preference for the species of shortest chain length. The simulations determined that the N and M dependences of probe motion are captured in three parameters: the probability of a probe−host entanglement, the average duration of an entanglement, and the average displacement of an entanglement. Hosts exert their greatest impact on probe motion when N and M (measured in chain length) are approximately equal.

A system employing nearly monodisperse hosts offers at least four benefits to a study of CE separation mechanisms. First, the meaning of dilute for hosts is straightforward; i.e., c needs only to fall below c^*, a well-defined threshold. While this threshold can be reasonably estimated from intrinsic viscosity or light scattering data, how one should define or measure c^* in a polydisperse host system (i.e., with PDI greater than 1.2) is far less obvious. Second, in a sufficiently dilute solution of probes and hosts, separation can be explained solely in terms of binary interactions between probe and host. In this limit, host-induced attenuation of probe motion should be proportional to c, a feature allowing independent examination of concentration and molecular weight effects. Third, assuming hosts and probes possess comparable local chain configurations, the separation becomes symmetrical: after reversing the identity of probe and host, an observer moving at the average probe velocity will observe the same dynamics as a stationary observer. In molecular modeling, this symmetry allows probe and host to be treated equivalently. Fourth, the set of chain−chain interactions in a system of monodisperse probes and hosts is the simplest one possible. One can learn by experiment how each probe−host chain length combination behaves; in a polydisperse host system, one cannot directly determine the modulation of probe chains of size M by host chains of size N.

A significant number of PSS and pullulan fractions with PDIs below 1.2 are available in the molecular weight range between 5000 and 2 000 000. These linear polymers display comparable persistence lengths, ≈2−3 nm for PSS (in the electrolyte of interest)[31] and ≈1.6 nm for pullulan.[32−34] Because the two polymers possess somewhat different mass per chain lengths, 820 and 320 g/(nm mol), respectively, a pullulan chain is approximately 2.5 times longer than a PSS chain of the same molecular weight. Pullulan's large configurational freedom relative to polysaccharides of similar structure (i.e., amylose) has been traced to the α-1,6-glucosidic linkages between the polymer's maltotriose repeat units. PSS and pullulan do not associate with each other, water is a good solvent for both, and the two do not appreciably bind to the walls of fused silica CE capillaries. A previous investigation employed pullulan at c much above c^* to implement a CE separation of SDS−protein complexes.[35,36]

Our probe−host system is in many ways chemically and structurally similar to the more familiar system of DNA−hydroxyethylcellulose. However, caution is advised in directly comparing our system to any other. For example, by focusing on a single probe−host combination, the current study cannot elucidate the role of chain stiffness on the probe−host interaction. DNA (persistence length ≈ 45 nm) and hydroyethylcellulose (persistence length ≈ 8.3 nm) are relatively much stiffer than PSS and pullulan. Also, complicated trends in μ with salt concentration may be anticipated for a flexible probe such as PSS, which stiffens and swells at low salt.[31,37] Trends in salt dependence for an inherently stiff polymer such as DNA may be simpler. Notwithstanding our recognition of these and other unexplored effects, we believe that a single basic interaction mechanism can unify and explain, at least in qualitative terms, how probe separation is achieved in the dilute host environment.

Experimental Section

Instrumentation. Fused silica capillaries of 50 μm internal diameter (Polymicro Technologies) are cut to 60 cm lengths, and a window through the outer polyimide coating is etched in each to create a 40 cm capillary test section. Except as noted, a 30 kV power supply (Glassman High Voltage, Inc.) adjusted to 15 kV drives solute motion. This voltage creates in the capillary a nominal electric field E of 250 V/cm. The capillary and electrode vials are kept inside an interlocked, temperature-controlled Plexiglas housing at 20 ± 1 °C. An absorbance detector (ISCO model CV^4) operating at 235 nm measures PSS concentration at the window; pullulan, present in both electrode vials and throughout the capillary, does not absorb at this wavelength.

Materials. Low-polydispersity PSS probes with M between 3×10^4 and 1.2×10^6 are purchased from a commercial vendor (Scientific Polymer Products). These probes are identified in electropherograms by numbers **1**−**7**, assigned in order of decreasing M. Likewise, low-polydispersity pullulan hosts with N between 2×10^4 and 1.7×10^6 are purchased from a second vendor (Showa Denko Shodex Standard kit P-82 available through Phenomenex). Table 1 presents relevant probe and host properties as described by the two vendors. A single free solution electrophoresis experiment employs a smaller PSS of M equal to 5.0×10^3 (Scientific Polymer Products).

Hosts are dissolved in prefiltered (0.22 μm), 0.01 M dibasic sodium phosphate electrolyte (pH ≈ 9.2, ionic strength ≈ 0.03M) at c equal to c^* or $2c^*$ and then diluted with the same electrolyte to the desired test concentration. Mechanical agitation is avoided during handling of host solutions, and to ensure homogeneity, the solutions are stored prior to use for at least 48 h in a refrigerator. Values of c^*, which scale c throughout this presentation, are calculated from literature light scattering or viscosity data[32] using either $c^* = N/[(4/3)\pi R_g^3]$ or $c^* \approx [\eta]^{-1}$, where R_g is the radius of gyration and $[\eta]$ is the intrinsic viscosity. Table 1 lists nominal c^* values for each pullulan fraction. Because host solutions are dilute, their relative viscosity can be accurately estimated as $1 + c/c^*$.

The PSS test solutions, often combining several molecular weight fractions, are prepared at a total PSS concentration of 1.00×10^{-3} g/ cm^3 in small, separated portions of the host solution; this concentration lies below all PSS critical overlap concentrations. Addition to the test solutions of a small concentration of the neutral, UV-absorbing compound benzyl

Table 1. Probe and Host Properties

Probe			
molecular weight, M	PDI	chain length (nm)	sample designation
1.188×10^6	1.17	14.5×10^2	1
8.01×10^5	1.16	9.77×10^2	2
5.05×10^5	1.24	6.16×10^2	3
2.62×10^5	1.10	3.20×10^2	4
1.04×10^5	1.20	1.27×10^2	5
5.7×10^4	1.05	0.69×10^2	6
3.1×10^4	1.35	0.38×10^2	7

Host			
molecular weight, N	PDI	chain length (nm)	c^* (g/cm^3)
1.66×10^6	1.14	51.9×10^2	3.5×10^{-3}
8.53×10^5	1.14	26.7×10^2	5.6×10^{-3}
3.80×10^5	1.12	11.9×10^2	1.3×10^{-2}
1.86×10^5	1.13	5.81×10^2	1.6×10^{-2}
1.00×10^5	1.10	3.13×10^2	2.2×10^{-2}
4.80×10^4	1.09	1.50×10^2	3.4×10^{-2}
2.37×10^4	1.07	0.74×10^2	5.1×10^{-2}

alcohol permits tracking of the electroosmotic flow velocity in the capillary.

Procedures. New capillaries are sequentially treated with 1 M NaOH (several hours), 0.1 M NaOH (10 min), and 0.01 M NaOH (10 min), steps that clean the capillary walls and expose the maximum density of siloxy groups. After rinsing with host-free electrolyte, host solutions are injected into the capillary, and the voltage is applied until current and absorbance stabilize. As needed subsequently, capillaries are reconditioned with 1 M NaOH (10 min); reconditioning is suggested when problems of reproducibility, current variation, or baseline fluctuation arise. Capillaries are stored overnight in 0.001 M NaOH.

An experiment begins with a 6 s electrokinetic injection of the probe solution at the anodic end of the capillary. After injection, this end is returned to a source vial containing a solution of hosts in electrolyte, and the voltage is reapplied. Electrophoretic velocities are obtained by subtracting the probe velocity from the electroosmotic flow velocity; the latter can be unambiguously determined from electropherogram peak positions of polymer and benzyl alcohol. Injection at the capillary's anodic end manifests the dominance of electroosmotic flow over electrophoretic migration. For the range of experimental conditions employed, μ is determined to an accuracy of ±3% or better. Dilution of the PSS samples to lower PSS concentration does not affect either the shape or position of electropherogram peaks, suggesting the absence of significant anomalies from electromigration dispersion. This type of dispersion arises when the conductivity of the injected sample does not closely match the conductivity of the run electrolyte. While PSS does not adsorb to the capillary walls, an unexpectedly large reduction of the electroosmotic flow velocity at larger c suggests that weak, reversible binding of pullulan may occur. (Electroosmotic flow recovers slowly after pullulan is eliminated from the electrolyte.) Because of this flow reduction, the current study's protocols will not suffice at higher c (i.e., when c exceeds c^* for low N pullulans).

Results and Discussion

Complications. Although the goal is to understand how N and M affect μ in the dilute host regime, these chain length dependences cannot be isolated as ideally as we would desire by experiment. Three complicating factors will thus be discussed before the presentation of the main findings.

Our earlier Monte Carlo simulations[29,30] found that field-induced chain distortions probably dominate the dynamics of probe−host interaction. Chain distortion under CE conditions has been observed for large DNA molecules by electric birefringence, dichroism, and fluorescence microscopy.[25−28] In the presence of chain distortions, μ might be expected to vary with E. Figure 1a shows data from of CE experiments designed to assess the dependence of μ on E. These data summarize how E affects the motion of $M = 1.04 \times 10^5$ and 5.05×10^5 probes in free solution (i.e., in the absence of hosts) and in a solution of $N = 3.8 \times 10^5$ hosts at $c/c^* = 0.25$. As expected, the free solution experiment does not distinguish the two probes, a trend consistent with the known M independence (at high M) of the free solution mobility μ_0. The same data imply an increase in μ_0 for E above 250 V/cm. This increase, however, is an artifact of incomplete suppression of Joule heating. Less than ideal heat dissipation causes the capillary interior to rise above the target temperature, and as a result, the medium viscosity drops; the net consequence is an enhanced value of the apparent μ_0. In accord with this explanation, the current in the capillary rises linearly to 9 μA at 250 V/cm, while above this field strength the current rise nonlinearly.

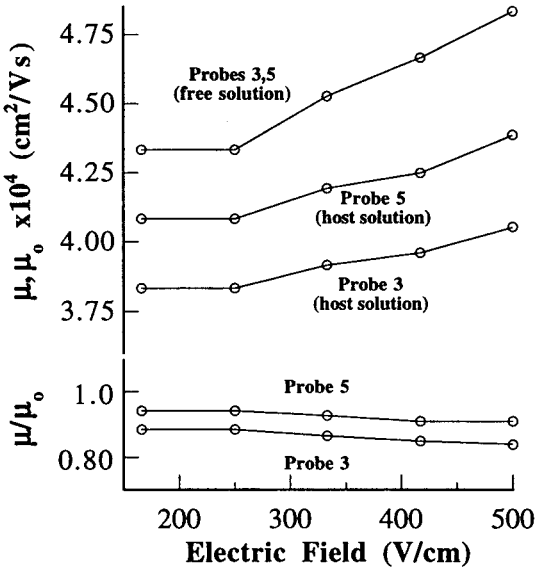

Figure 1. E dependence of μ and μ_0 for two PSS probes varying in M. As shown at the top, addition of $N = 380\,000$ pullulan hosts at $c^*/4$ reduces μ in an M-dependent manner from its M-independent value μ_0 in free solution. At the bottom, the ratio μ/μ_0 for the same experiments is plotted against E.

For a system containing hosts, the same figure reveals a comparable increase of μ with E. In this case, M clearly affects the attenuated value of μ, with the larger probe's motion reduced more significantly by hosts. With hosts present, the reason(s) for the rise of μ with E are less clear, as chain distortions of the type monitored by simulation and birefringence might explain the observed trend. Chain distortions apparently explain the field-dependent mobilities noted when large DNA probes migrate in semidilute and concentrated host solutions.[3,19] To clarify, Figure 1b displays the mobility ratio μ/μ_0 as a function of E for the same dilute host systems. As the presence or absence of hosts does not affect heat dissipation (the current in the capillary is essentially unaffected by the presence of hosts), this plotting scheme suppresses heat-transfer artifacts. The resulting normalized mobility curves are nearly flat, strongly suggesting that E does not directly alter μ in the dilute host regime at the M or E values examined. This unexplained trend (similarly seen for DNA at intermediate/low E and/or M[19]) simplifies subsequent experi-

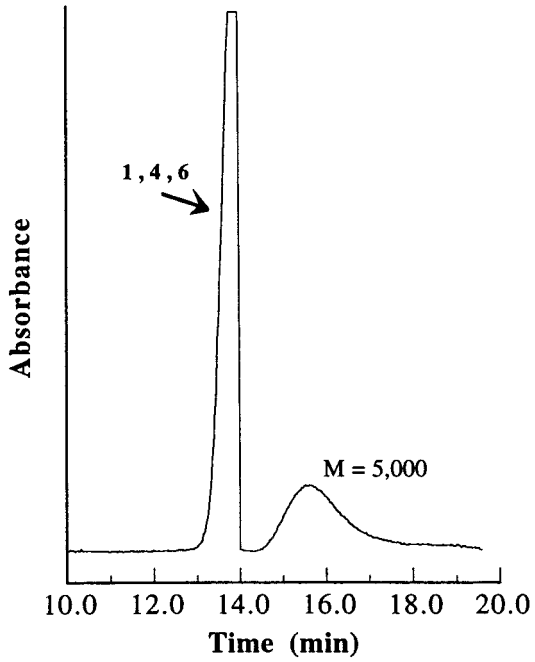

Figure 2. Raw free solution electropherogram for a mixture of four PSS probes varying in M.

ments, allowing E to be adjusted to a single nominal value, 250 V/cm, which maintains the capillary interior at constant temperature. Further work on the E dependence of μ appears warranted, as the trend seen in Figure 1b could be associated with either a high E or a low E plateau in μ, behaviors respectively associated with highly distorted or undistorted chain configurations. (More rigorous controlling of the temperature rise with E might seem a better way to study the impact of chain distortion on μ than plotting the ratio μ/μ_0. The mobility ratio approach, however, allows assessments of E dependence at much higher E, even into the regime where a temperature rise cannot be avoided.)

The second complication involves the M dependence of μ_0. Below a critical M value, μ_0 becomes M dependent. Figure 2 presents a raw free solution electropherogram illustrating the consequence of this dependence. In our system, with electroosmotic flow dominant, substances of larger μ_0 elute at later time. The initial (sharp) peak corresponds to three high M polymers not distinguished from each other by free solution CE. The second (broad) peak, at larger μ_0, corresponds to an easily distinguished fraction of lower M ($M \approx 5000$). The onset of free solution M independence for this polymer/electrolyte system is not accurately known, although the transition lies near M ≈ 20 000. As has been reported elsewhere,[38] the departure of μ_0 from M independence for flexible polyelectrolytes differs from that predicted by simple theory, with μ_0 passing at lower M through an unexpected maximum, a feature explaining the general appearance of Figure 2. When studying probe separation by hosts, we avoid this poorly understood complication by examining samples from the range $M > 30\,000$.

The third complication is the true definition of "dilute" for a system of well-defined hosts and probes. By dilute, we intend to imply a system with dynamics dominated by binary configurational interactions between otherwise isolated chains. A system combining dilute probes and dilute hosts may not fit this strict definition of dilute; for $M \gg N$, the domain of a single large probe may be able to span between the domains of smaller yet nonoverlapping hosts, while for $M \ll N$, the domain of a single large host may be able to span between the domains of smaller yet nonoverlapping probes. The latter case does not present an issue in this study since the probes are always present at concentrations much below c^*. Dominance of binary probe−host interactions in a probe−host mixture defines a new concentration threshold c'. Representing probe and host by their respective radii of gyration R_M and R_N, and ignoring possible order unity prefactors, we can write for the case $R_M \gg R_N$

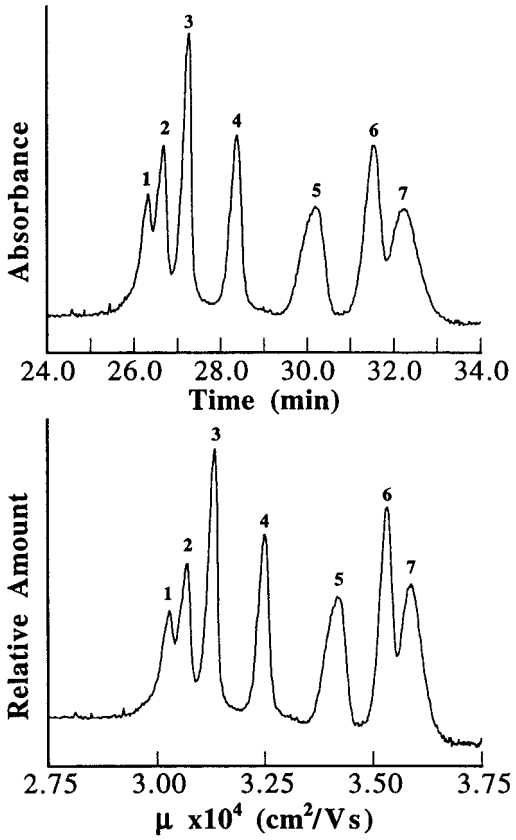

Figure 3. Transformation of a raw electropherogram (a) into a μ distribution (b). All seven of the PSS probes of Table 1 are separated and identified in a dilute solution containing $N =$ 380 000 hosts at $c^*/2$. The field E is 80 V/cm.

$$c' \approx \frac{N}{\frac{4}{3}\pi {R_N}^3 N_a \left[1 + \frac{R_M}{R_N}\right]^3} \qquad (1)$$

where N_a is the Avogardro constant. Less than c^* by the added factor in the denominator, c' varies with both N and M. In the extreme cases of the current study, c' calculated by this formula is roughly a factor of 3 smaller than c^*. Some of the experiments we report fall into the gap between c' and c^*. The mobility controlling chain interactions in the range $c' < c < c^*$ will be more complex than those at $c < c'$, for example, possibly involving the sort of higher-order interaction dynamics modeled by Hubert et al.[24]

Electropherograms. Electropherograms recorded in the presence of host polymers appear similar to those produced by size exclusion chromatography, with high M probes eluting first. Figure 3a displays a typical absorbance vs time trace for a mixture of the seven PSS probes listed in Table 1. In this example, the capillary

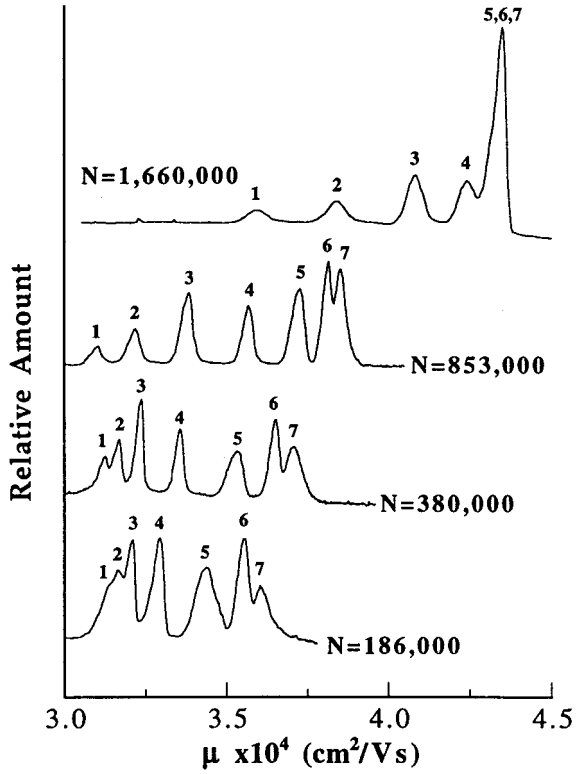

Figure 4. Influence of N on μ distributions for a seven-component probe mixture. Hosts are present at $c = c^*/2$ in each case.

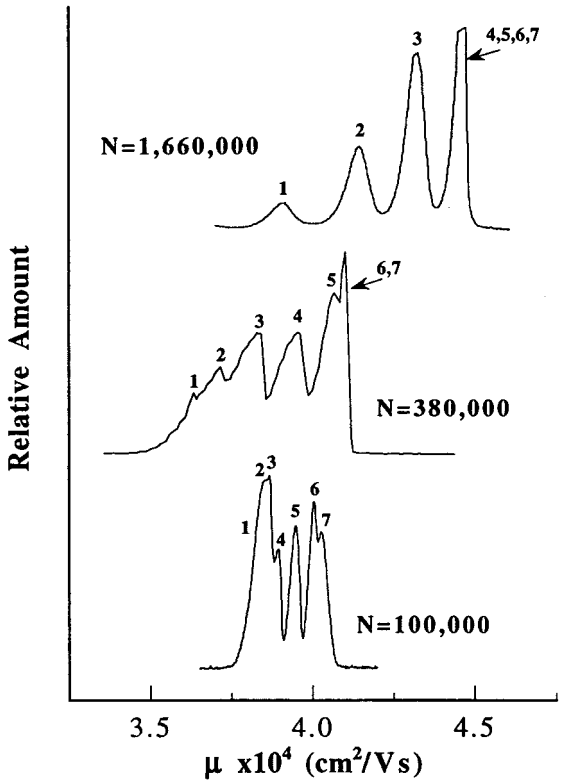

Figure 5. Influence of N on μ distributions for a seven-component probe mixture. In each case, $c = c^*/4$.

contains $N = 380\,000$ hosts at $c^*/2$, and the applied field is 80 V/cm. The most striking feature of such electropherograms is the peak resolution: in some cases, M differences as small as 20−25% lead to baseline level separation. This resolution far surpasses that of ordinary chromatographic techniques and, at higher M, approaches levels otherwise obtainable only through gel electrophoresis. Many previous investigators using CE in neutral polymer solutions have reported polyelectrolyte separations of comparable quality.[4,6,8,11,12,14,15,19,36]

In addition to easily adjustable parameters such as electric field strength and capillary length, the appearance of a raw CE electropherogram reflects the electroosmotic flow velocity, a quantity difficult to hold constant from run to run. CE results presented in terms of μ, or the distribution of μ in the case of multicomponent samples, are more readily evaluated and universal. Data in this study are thus transformed into μ distributions using the electroosmotic flow velocity determined via the neutral marker. The transformation is analogous to the calculation of a molecular weight distribution from a size exclusion chromatography trace. Figure 3b displays the mobility distribution calculated from the data of Figure 3a. Long PSS chains in the host-free electrolyte possess a mobility of $(4.5 \pm 0.1) \times 10^{-4}$ cm^2/(V s), so depending on M and N, the host polymers in this experiment attenuated PSS probe motion by 15−30%. When overlap of peaks occasionally confuses determination of component mobilities for a probe mixture, the individual probe species are rerun separately to eliminate the confusion.

We believe that the breadth of many of these PSS probe peaks manifests true sample polydispersity rather than peak-broadening processes. However, in the absence of an accurate and independent measure of polydispersity, this belief cannot be confirmed. Accepting our conjecture, the PDI values inferred from the breadth of the peaks in Figure 3 fall roughly in the range 1.01−1.05. These values lie somewhat below the manufacturer-provided values presented in Table 1, but we have often found such manufacturer values for PDI to be only approximate. A subsequent paper will rigorously evaluate the suitability of the new electrophoretic approach for the measurement of synthetic polymer molecular weight distribution, comparing results by the current method to those from another, more established method. We feel confident that at high probe molecular weight the electrophoretic method will prove competitive or superior to alternatives.

Figure 4 illustrates the influence of N on probe separation at $c = c^*/2$. Comparing distributions, one immediately notes that larger probes are better separated at large N and smaller probes are better separated at small N, trends in accord with experimental results reported by other investigators. The best peak separation occurs when probe and host chain lengths are roughly the same. By comparing μ at c fixed relative to c^*, as done here, rather complex trends in probe peak position are created. For example, tracking the peak associated with the longest probe (**1**), the initial shift with increasing N is toward lower μ, but the trend eventually reverses at higher N and μ then grows. On the other hand, μ for the smallest probe (**7**) increases monotonically with N. Most of the improvement in peak resolution with N can be explained as a shift of smaller probes toward higher μ rather than enhanced attenuation of larger probes. If c rather than c/c^* were fixed, these trends with N would be different.

As expected in this dilute host regime, the quality of probe separation declines at lower c. This trend can be readily discerned in Figure 5, which presents results similar to those of Figure 4 but with c lowered to $c^*/4$.

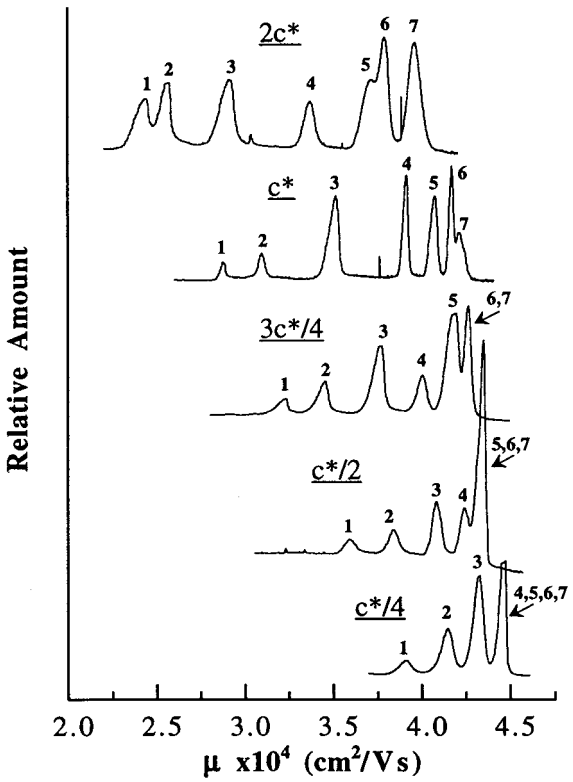

Figure 6. Influence of c on μ distributions for a seven-component probe mixture. In each case, $N = 1\ 660\ 000$.

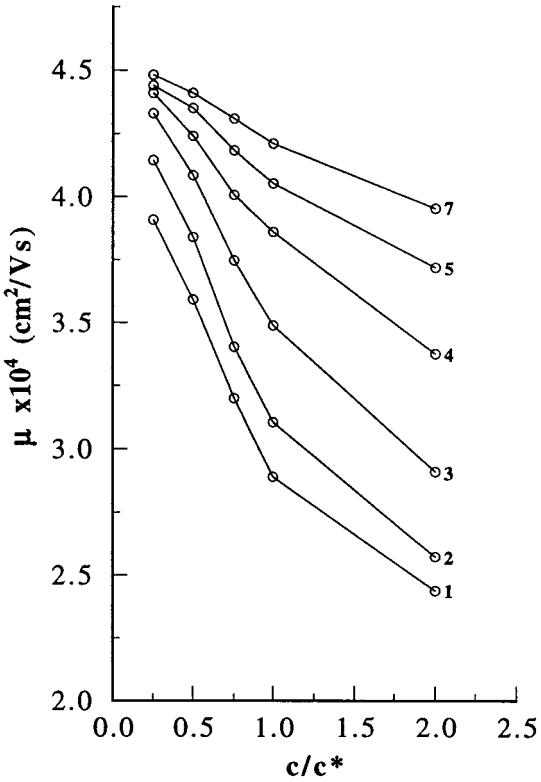

Figure 7. Dependence of μ on c/c^* for $N = 1\ 660\ 000$. (Data from probe 6 deleted for clarity.)

The spread of μ is now smaller and shifted upward in μ. One notes a loss of peak resolution even though μ remains substantially below μ_0; i.e., hosts can attenuate probe motion substantially even when this attenuation is not highly M dependent.

Figure 6 presents μ distributions for the same PSS probe mixture as Figure 4 but with N fixed and c varied relative to c^*. The fixed value of N is 1 660 000. One clearly observes increasingly hindered probe motion as c/c^* grows. Although the hindrance roughly grows with M, there is an intermediate window of M where c has the greatest impact. A careful examination, for instance, shows a reduced peak separation for the two highest M probes as c rises from c^* to $2c^*$. (This run is the only one undertaken at c greater than c^*.) Experiments with starting mixtures containing fewer than seven probes aid in the identification of peak positions when peak overlap occurs, e.g., for the low M probes of Figures 4−6.

Analysis of Trends with Host Concentration. The general appearance of Figure 6 suggests an approximately linear influence of c on μ, i.e., that at low values of c, μ is reduced from its free solution value μ_{o0} in proportion to the density of hosts present,

$$\mu = \mu_0 - f(M,N)\frac{c}{c^*} \qquad (2)$$

where $f(M,N)$ is a function independent of c. This form would be expected for probe motion at small E in a sufficiently dilute host matrix. To test the hypothesis, Figure 7 plots μ against c/c^* with M as a parameter; N is again fixed at 1 660 000. This plot roughly conforms to eq 2 at low values of c/c^*. Linear extrapolation of the different curves to zero c produces a universal intercept nearly equal to the independently measured value of μ_0. Concentration studies for this probe mixture using shorter host chains provide plots qualitatively similar to Figure 7, again with intercepts lying near μ_0.

The onset point for curvature in these data sets implies that hosts behave as dilute only when c falls below c^*. In addition, upward curvature reveals that concentrated, possibly entangled host chains attenuate probe motion less effectively (per chain) than physically isolated host chains (although the actual discrimination by mobility is better at or above c^*). Trends with M in the onset of curvature suggest, as argued earlier, that the threshold for dilute host behavior at fixed N is larger when probes are larger. The general appearance of Figure 7 is reminiscent of plots of μ vs c for dilute gels. However, the separation mechanisms in the two cases are obviously different, as are the magnitudes of E applied. In a dilute and polydisperse host solution, DNA displays a similar dependence of μ on c.[21,39]

The conjectured crossover to a new dynamics at c' cannot be verified from Figure 7, inasmuch as there are no obvious nonlinearities in any of the data sets for c less than c^*. The most obvious spot to search for a crossover corresponding to c' would be the figure's lowest curve, corresponding to the largest M probe; in this particular case, we predict from eq 1 that c' could be several times smaller than c^*. If so, near c' we would expect to observe the beginnings of upward curvature with increasing c. The trend would reflect the lower effectiveness in retarding probe motion of a second entangled chain of the dilute host solution, an effect predicted through the model of Hubert et al.[24] However, this type of behavior is not seen. The only obvious upward break in any of the figure's curves corresponds closely to c^*. Because eq 1 and the model of Hubert et al. involve several poorly known prefactors, difficulty in verifying the presence of a crossover at c' is not surprising.

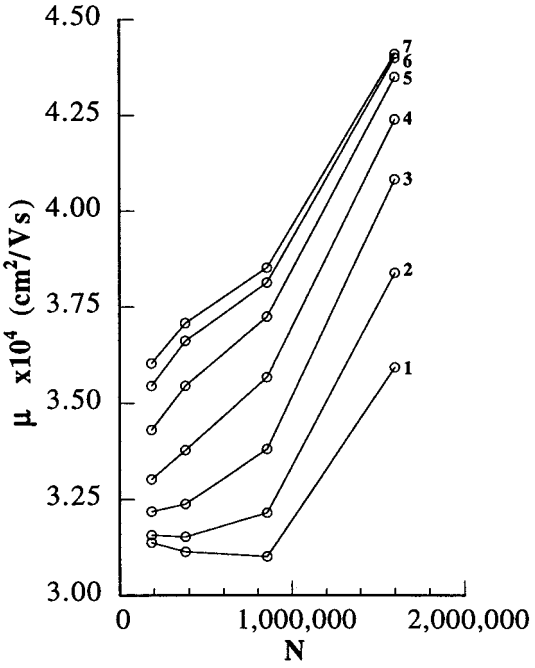

Figure 8. Dependence of μ on N for $c = c^*/2$. (Figure 9 plots two additional points for probe 1.)

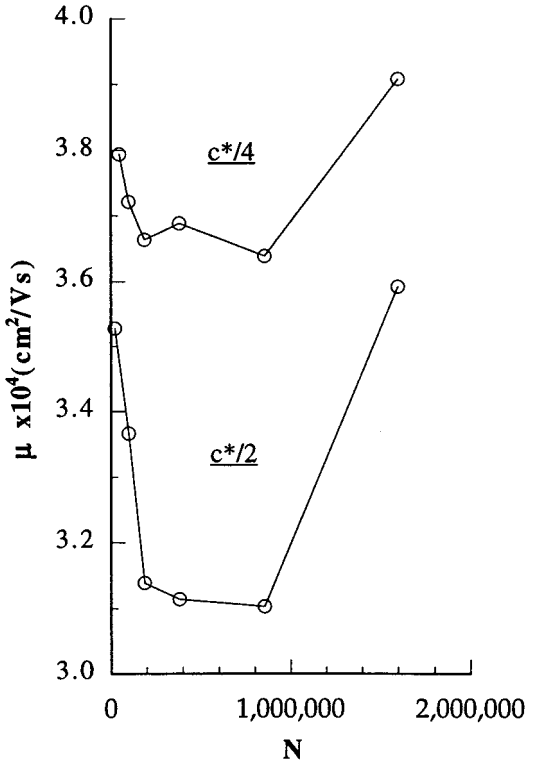

Figure 9. Dependence of μ on N for $M = 1\ 188\ 000$ (probe 1). (For clarity, two points on the bottom curve were not plotted in Figure 8.)

Analysis of Trends with Host Chain Length. Figures 4 and 5 reveal a complex dependence of μ on N. These trends are perhaps best appreciated by plotting μ vs N with either c/c^* or M held constant, as done in Figures 8 and 9, respectively. Figure 8 rigorously establishes two interrelated trends suggested several times in the literature and mentioned in the Introduction, that larger hosts better separate larger probes and that smaller hosts better separate smaller probes. These features are manifested in the bunching of curves in the upper right and lower left of Figure 8. Only by studying probe separation in nearly monodisperse host solutions, as done here, can these important trends be proven. Because μ cannot exceed μ_0, the curves of Figure 8 must converge at $\mu \approx \mu_0 \approx 4.5 \times 10^{-4}$ cm^2/(V s) for some larger value of N than studied here. The convergence can be attributed to the diminishing value of c^* as N becomes larger; if c rather than c/c^* were held fixed in this plot, no convergence would be observed.

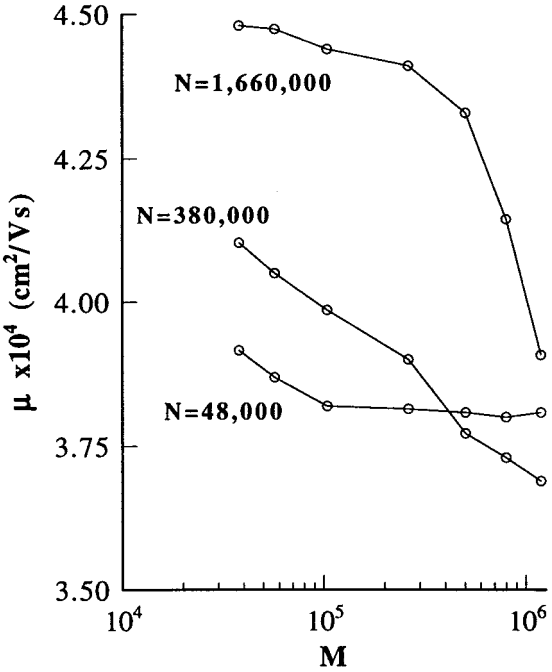

Figure 10. Dependence of μ on M for three hosts of different N present at $c = c^*/4$.

One interesting feature of Figure 8 is a minimum in the lowest curve, which plots data for the largest probe. This minimum was previously noted in the discussion of the complicated separation behavior of the low μ (high M) peaks in Figure 4. Figure 9, which plots additional μ data for this probe at fixed host concentrations of $c^*/2$ and $c^*/4$, shows this minimum more clearly and confirms that a similar minimum occurs at the lower host concentration. For both concentrations, the rather broad minimum roughly centers at $N = 500\ 000$. A pullulan chain of this molecular weight possesses a contour length approximately equal to that of a PSS chain of molecular weight $M = 1\ 250\ 000$. As discussed shortly, we believe that the near equality of probe and host chain lengths at the minimum is not a coincidence.

Analysis of Trends with Probe Chain Length. Figures 10 and 11 plot μ vs M while respectively holding either c/c^* (=0.25) or N (=1 660 000) constant. In the figure's semilog format, three regimes can be identified. Crudely, when $M \ll N$, probe−host interaction displays little M discrimination and μ approaches μ_0. The low M portion of the top curve best represents this regime. When $M \approx N$ (again, in crude terms only), μ falls rapidly with M, passing an inflection point. The middle curve reflects this intermediate regime, as do limited regions of the top and bottom curves. Finally, when $M \gg N$, μ asymptotically attains an apparent low plateau value dependent on N. In this limit, discrimination by M is once again poor or nonexistent. Unfortunately, the range of M available in this study is not sufficient for all three regimes to be observed at a single value of N.

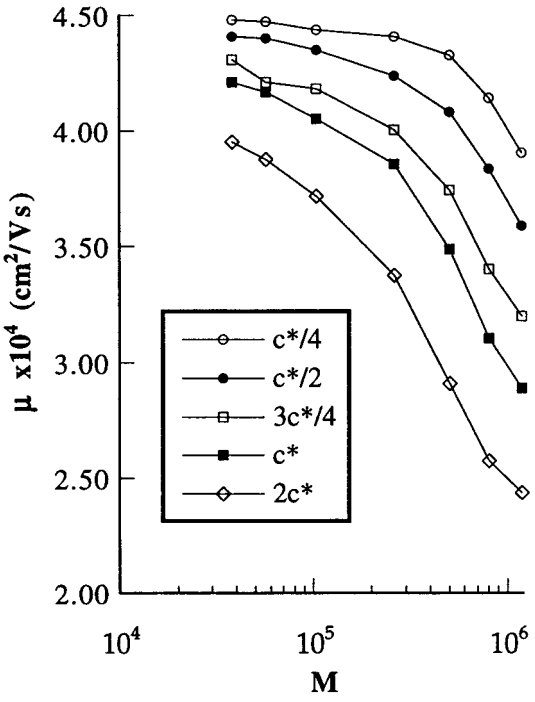

Figure 11. Dependence of μ on M for $N = 1\,660\,000$ hosts present at various values of c/c^*.

Holding N rather than c constant, Figure 11 reveals the same three mobility regimes as c is varied. Although none of the curves reach the anticipated final μ plateau, the approach to the third regime with increasing M can be clearly discerned through the inflections in the lower curves. Even when c exceeds c^*, the three regime curve shape is maintained. The main impact of c variations appears to be a shift of the inflection point to lower M as c increases. At $c > c^*$, this shift appears to lower the inflection below the condition associated with the equality of chain lengths for probe and host. Given the breaks in slope observed near c^* in Figure 7, the similarity in curve shape above and below c^* is surprising. We know from Figure 7 that the mechanisms of separation must change upon entering the semidilute host range.

Mechanism of Probe Separation in a Dilute Host Solution. The probe−host interaction dynamics uncovered in our previous Monte Carlo simulations[29] can explain much of the experimental data found in this paper. A single flexible charged probe released upfield from a single flexible neutral host was observed by simulation to drift into the host and eventually to entangle. For the vast majority of probe releases, a hairpin-like entanglement formed, with the two free probe segments on either side of the locus of entanglement extending downfield. During the entanglement and subsequent dragging of the coupled probe−host complex downfield, the host developed a similar configuration but with its two free segments extending upfield. This double-hairpin entanglement persisted until one of the free host or probe segments fluctuated through the locus of entanglement, destroying the coupling between probe and host motions. The simulations did not vary c, so in this respect they provide no guidance into the probe−host dynamics. However, from experiment one can infer that variation of c below c^* basically modulates the average frequency of encounter between probe and host. The consequence is a drop of μ below μ_0 in proportion to c.

Interestingly, while the spread of μ with M always increases for $c < c^*$ (i.e., higher host density always improves discrimination by probes size), the same trend is not followed near and above c^*. The reversal of trends with c is most obvious in the bottom two curves of Figure 7, which reveal that the separation between the two largest probes declines as c rises from c^* to $2c^*$. This concentration effect, first noticed by Barron et al.[21] for DNA separation in solutions of hydroxyethylcellulose, emphasizes the difference between dilute and semidilute host solutions. In the latter environment, the interaction between host chains apparently interferes with the molecular weight sensitivity of 1−1 probe−host entanglement. As Barron et al. also found, this concentration crossover first impacts the separation of the larger probes. Discrimination of the smaller probes continues to improve for c in excess of c^*. Although our data are limited, we speculate that for $M > N$ discrimination by μ weakens as host concentrations enter the semidilute regime.

Even focusing on the dilute regime, the influence of N on μ is not straightforward. To explain this influence in our previous simulation study, we identified three separate physical effects: the probability of probe−host entanglement during an encounter (effectively a collision cross section), the average duration of a probe−host entanglement, and the average spatial displacement of probe and host during an entanglement. The same effects can be used to explain much of our N-dependent μ data, especially the data's most distinctive feature, the minima noted in Figure 9. For $N \ll M$, a migrating probe effectively drags an entangled host downfield, since the added friction from the accompanying host is small. The drag on the entangled probe−host complex increases with N across this range, lowering μ. Above a threshold N value, however, the dragging ceases to dominate probe motion, and the frequency and average duration of entanglement begin to exert a larger impact on a probe's average motion. Because c/c^* is fixed, increases of N at high N eventually lead to fewer probe−host collisions, albeit with somewhat greater average entanglement duration. The net outcome is an enhancement of μ. Figure 8 suggests that μ rises nearly to μ_0 at high N, although the rate of the rise is more gradual at larger M; the lessening of the rate of rise reflects an increase in average entanglement duration with N. Continuing to examine Figure 8, the convergence of μ at smaller N can be explained in terms of the lack of M discrimination when $N \ll M$. In the limit of very small N, the hosts simply viscosify the solution, equally reducing μ from μ_0 for all probes. Stated differently, when hosts are much smaller than probes, probe−host collisions are relaxed entirely by host motions, eliminating any M dependence to μ. Nevertheless, the probe−host collisions still hinder probe motion, implying $\mu < \mu_0$.

The three regimes of M-dependent probe motion uncovered in Figures 10 and 11 can be explained by similar arguments. When $M \ll N$, collisions are infrequent, and although the average duration of these collisions is strongly M dependent, μ falls only slightly below μ_0, with discrimination of μ by M poor or nonexistent. As M increases, the duration of entanglement rises, and although collisions remain equally frequent, the duration of entanglement eventually controls μ. In this regime, the translation of an entangled probe−host complex is small, and with probes now entangled for a

large fraction of time, the capture and release of probes by essentially fixed hosts produces strongly *M*-dependent probe motion. For *M* greatly exceeding *N*, *M* discrimination again declines, as noted before in the lower *N* data of Figure 8. Large probes now move in a sea of smaller hosts, and fast, *M*-independent host motions relieve probe−host entanglements. By analogy to the low *N* behaviors displayed in Figure 9, we might expect that μ in Figures 10 and 11 would eventually rise at very large *M*; i.e., the μ plateau in these figures defining the third regime is only apparent, with the plateau actually corresponding to the bottom of the broad minima of the curves in Figure 9. A final rise remains hypothetical, as the behavior has not been observed by experiment. However, the simulations clearly show such a rise at large *M*. We do not expect μ to regain values strictly comparable to μ_0.

Summary

The mechanisms responsible for the effective CE separation of polyelectrolytes in a dilute neutral polymer solution have been explored through a systematic set of experiments employing model hosts and probes. An earlier simulation study identified probe−host interaction dynamics that can explain the variation of μ with *N*, *M*, and *c* seen in these experiments. Qualitatively, all major trends can be rationalized through the dynamics of pairwise collisions between probe and host. The interplay of *N* and *M* on the outcome of such collisions is complex, involving entanglement probabilities, probe−host displacements, and entanglement durations. However, all observed trends are in qualitative accord with expectation. Unfortunately, our understanding of effects of *E* variation on μ remain much poorer; specifically, knowledge of the relative levels of chain deformation and orientation for both probe and host would be useful in verifying the proposed chain dynamics. By transforming experimental data into absolute electrophoretic mobilities and by carefully controlling experimental conditions, this study should be of considerable help to future investigations attempting to predict, with no fitting parameters, electrophoretic motion from molecular structure. The results may also assist efforts to optimize polyelectrolyte separation conditions and to employ electrophoretic methods to examine more structurally complex probes or hosts.

Acknowledgment. Financial support for this project was from the National Science Foundation through the University of Massachusetts Materials Science and Engineering Center.

References and Notes

(1) Bode, H.-J. *Anal. Biochem.* **1977**, *83*, 364.
(2) Bode, H.-J. *Anal. Biochem.* **1979**, *92*, 99.
(3) Heiger, D. N.; Cohen, A. S.; Karger, B. L. *J. Chromatogr.* **1990**, *516*, 33.
(4) Poli, J. B.; Schure, M. R. *Anal. Chem.* **1992**, *64*, 896.
(5) Kleemiss, M. H.; Gilges, M.; Schomburg, G. *Electrophoresis* **1993**, *14*, 515.
(6) Chang, H.-T.; Yeung, E. S. *J. Chromatogr. B* **1995**, *669*, 113.
(7) Chiari, M.; Nesi, M.; Righetti, P. G. *J. Chromatogr. A* **1993**, *652*, 31.
(8) Barron, A. E.; Soane, D. S.; Blanch, H. W. *J. Chromatogr. A* **1993**, *652*, 3.
(9) Barron, A. E.; Sunada, W. M.; Blanch, H. W. *Electrophoresis* **1995**, *16*, 64.
(10) Sudor, J.; Novotny, M. V. *Anal. Chem.* **1994**, *66*, 2446.
(11) Clos, H. N.; Engelhardt, H. *J. Chromatogr. A* **1998**, *802*, 149.
(12) Kim, Y.; Morris, M. D. *Electrophoresis* **1996**, *17*, 152.
(13) Kim, Y.; Morris, M. D. *Anal. Chem.* **1994**, *66*, 3081.
(14) Minárik, M.; Gas, B.; Kenndler, E. *Electrophoresis* **1997**, *18*, 98.
(15) Cottet, H.; Gareil, P. *J. Chromatogr. A* **1997**, *772*, 369.
(16) Cottet, H.; Gareil, P.; Viovy, J.-L. *Electrophoresis* **1998**, *19*, 2151.
(17) Bünz, A. P.; Barron, A. E.; Prausnitz, J. M.; Blanch, H. W. *Ind. Eng. Chem. Res.* **1996**, *35*, 2900.
(18) Pulyaeva, H.; Wheeler, D.; Garner, M. M.; Chrambach, A. *Electrophoresis* **1992**, *13*, 608.
(19) Mitnik, L.; Salomé, L.; Viovy, J. L.; Heller, C. *J. Chromatogr. A* **1995**, *710*, 309.
(20) Barron, A. E.; Blanch, H. W.; Soane, D. S. *Electrophoresis* **1994**, *15*, 597.
(21) Barron, A. E.; Sunada, W. M.; Blanch, H. W. *Biotechnol. Bioeng.* **1996**, *52*, 259.
(22) Baba, Y.; Ishimaru, N.; Samata, K.; Tsuhako, M. *J. Chromatogr. A* **1993**, *653*, 329.
(23) Kim, Y.; Morris, M. D. *Anal. Chem.* **1995**, *67*, 784.
(24) Hubert, S. J.; Slater, G. W.; Viovy, J.-L. *Macromolecules* **1996**, *29*, 1006.
(25) Carlsson, C.; Larsson, A.; Jonsson, M.; Nordén, B. *J. Am. Chem. Soc.* **1995**, *117*, 3871.
(26) Shi, X.; Hammond, R. W.; Morris, M. D. *Anal. Chem.* **1995**, *67*, 1132.
(27) Carlsson, C.; Jonsson, M. *Macromolecules* **1996**, *29*, 7802.
(28) Starchev, K.; Sturm, J.; Weill, G. *Macromolecules* **1999**, *32*, 348.
(29) Starkweather, M. E.; Muthukumar, M.; Hoagland, D. A. *Macromolecules* **1998**, *31*, 5495.
(30) Starkweather, M. E.; Muthukumar, M.; Hoagland, D. A. *Macromolecules* **1999**, *32*, 6837.
(31) Wang, L.; Yu, H. *Macromolecules* **1988**, *21*, 3498.
(32) Kato, T.; Okamoto, T.; Tokuya, T.; Takahashi, A. *Biopolymers* **1982**, *21*, 1623.
(33) de Nooy, A. E. J.; Besemer, A. C.; van Bekkum, H.; van Dijk, J. A. P. P.; Smit, J. A. M. *Macromolecules* **1996**, *29*, 6541.
(34) Nishinari, K.; Kohyama, K.; Williams, P. A.; Phillips, G. O.; Burchard, W.; Ogino, K. *Macromolecules* **1991**, *24*, 5590.
(35) Nakatani, M.; Shibukawa, A.; Nakagawa, T. *Electrophoresis* **1996**, *17*, 1210.
(36) Nakatani, M.; Shibukawa, A.; Nakagawa, T. *J. Chromatogr. A* **1994**, *672*, 213.
(37) Smisek, D. L.; Hoagland, D. A. *Macromolecules* **1989**, *22*, 2270.
(38) Hoagland, D. A.; Arvanitidou, E.; Welch, C. *Macromolecules* **1999**, *32*, 6180.
(39) Grossman, P. D.; Soane, D. S. *Biopolymers* **1991**, *31*, 1221.

MA9911546